RSC Advances

PAPER

View Article Online
View Journal | View Issue

Cite this: *RSC Adv.*, 2022, **12**, 19270

AIE and reversible mechanofluorochromism characteristics of new imidazole-based donor–π–acceptor dyes†

Ohoud F. Al Sharif,[abcd] Laila M. Nhari,[e] Reda M. El-Shishtawy,*[a] Mohie E. M. Zayed[a] and Abdullah M. Asiri[af]

Four new imidazole-based donor–π–acceptor **2a–2d** dyes have been synthesized, and their solvatochromism, aggregation-induced emission (AIE) and mechanofluorochromic (MFC) properties were investigated. The new dyes **2a–2d** were designed to have 1,4,5-triphenyl-1*H*-imidazole as an electron donor (D) and 1-indanone, 1,3-indandione, 2-phenylacetonitrile and 2-thiopheneacetonitrile as electron acceptors (A) linked through a phenyl bridge. The maximum absorption wavelength of **2a–2d** dyes in DCM solution appeared at 376, 437, 368, and 375 nm, respectively. The dyes exhibit a high molar extinction coefficient (ε) and large Stokes shift, making them useful in optoelectronic applications. Solvatochromic properties of dyes **2a–2d** have been studied and showed bathochromic changes in emission wavelengths, from 449 to 550 nm for **2a**, 476 to 599 nm for **2b**, 438 to 520 nm for **2c**, and from 439 to 529 nm for **2d**, as the solvent polarity increased from *n*-hexane to acetonitrile. Moreover, in dioxane/water mixture systems, AIE behaviors were observed, and the emission intensity of **2b–2d** dyes increased by around 5, 3, and 3 times in the mixed solvent (dioxane : water = 10 : 90) in contrast to pure dioxane. In addition, the XRD data of the **2a–2d** dyes in pristine, ground, and fumed states illustrate that the transition between the ordered crystalline and disordered amorphous phases is the primary cause of MFC behaviors mechanism. Density functional theory (DFT) and time-dependent density functional theory (TD-DFT) showed that the highest occupied molecular orbital (HOMO) of dyes is distributed on the donor unit. In contrast, the lowest unoccupied molecular orbital (LUMO) is mainly placed on the acceptor unit to reveal that the HOMO–LUMO transition has a great ICT character.

Received 5th March 2022
Accepted 21st June 2022

DOI: 10.1039/d2ra01466a

rsc.li/rsc-advances

1. Introduction

As an attractive research topic, solid-state emitters and molecular smart materials have a lot of advantages in current technology and optoelectronic device advancements such as organic light-emitting diodes (OLEDs),[1,2] fluorescent sensors,[3] data storage, and security printing.[4] Specifically, mechanofluorochromic (MFC) materials, in which their solid-state fluorescence colors display noticeable changes in response to external force, have gained great attention. The MFC innovative materials have shown advanced application in different fields, such as mechanosensing, wearable devices, anti-counterfeiting, optical recording, security papers, data storage, and optoelectronics.[5–13] Regrettably, most classic emissive materials emit intense light in dilute solutions. However, this bright luminescence is often attenuated or quenched at high concentrations, in a phenomenon known as aggregation-caused quenching (ACQ). Moreover, the ACQ effect significantly impedes the use of high-performance mechanical force-responsive materials.[14–18] Interestingly, the aggregation-induced emission (AIE) phenomenon is caused by the restricted intramolecular movements.[17,18] AIE-active fluorogenic compounds (AIEgens) can overcome ACQ and provide robust solid-state emission.[19,20] This fascinating feature of AIEgens has prompted researchers to explore their potential uses in various optoelectronic devices,[21–25] sensors,[26–28] photodynamic therapy,[29] and biological applications.[30,31] Importantly, imidazole derivatives are considered good candidates as AIEgens.[32]

Organic D–π–A systems have remarkable optical and spectral properties due to their highly polarizable structures resulting from efficient ICT from the donor to the acceptor.[33–38] Consequently, ICT compounds have been earned substantial research interest owing to their potential application in

[a]*Chemistry Department, Faculty of Science, King Abdulaziz University, Jeddah, Saudi Arabia. E-mail: relshishtawy@kau.edu.sa*
[b]*King Fahd Center for Medical Research, King Abdulaziz University, Jeddah, Saudi Arabia*
[c]*Center of Nanotechnology, King Abdul Aziz University, Jeddah 21589, Saudi Arabia*
[d]*Department of Chemistry, College of Science, Taif University, Taif, Saudi Arabia*
[e]*Chemistry Department, Faculty of Science, University of Jeddah, Jeddah, Saudi Arabia*
[f]*Center of Excellence for Advanced Materials Research, King Abdulaziz University, Jeddah 21589, Saudi Arabia*

† Electronic supplementary information (ESI) available. See https://doi.org/10.1039/d2ra01466a

chemical sensing,[39–42] nonlinear optical (NLO) materials,[43–46] optoelectronic devices,[47] dye-sensitized solar cells,[48–53] and organic light-emitting diodes (OLEDs)[54,55] with large Stokes shift and dipole moment in the excited state.[56]

Significantly, substituted imidazole derivatives have been of major interest in the production of novel materials for opto-electronic applications.[35] Also, small organic molecules with a highly substituted imidazole moiety as an electron donor with different acceptors have scarcely been published.[57]

The majority of the newly produced mechanofluorochromic (MFC) materials as ICT dyes with AIEactive features, together with their simple synthetic techniques, have revealed that small organic molecules as AIEactive materials are preferred over large structures.[1] Also, D–π–A organic frameworks were used to obtain emissive solid-state materials that exhibited MFC behavior.[58]

In 2017, Tang and co-workers reported the synthesis and optical properties of a D–π–A system of a tetraphenyl imidazole derivative (TIBM) that showed good AIEE-active properties.[59] Albeit this study is very interesting, studying the relationship between optical properties of tetraphenyl imidazole derivatives and the effect of different π-conjugated bridges and variety of electron acceptors is quite rare. Also, introducing variation of electron acceptors to AIE-active tetraphenyl imidazole derivatives is an effective synthetic strategy to obtain efficient tunable solid-state luminescent materials,[32] and will be a great choice to enhance MFC properties that provides most requirements mentioned above.

Keeping this in mind, herein we designed and synthesized small molecular systems having a 1,4,5-triphenyl-1*H*-imidazole moiety linked to four different acceptors, namely, indanone, indandione, 2-phenylacetonitrile, and 2-thiopheneacetonitrile **2a–2d**. One and two carbonyl withdrawing groups in indanone and indandione moieties, respectively, enhance the dielectric constant due to their strong polarity. Otherwise, the cyano group in α-cyanostilbene moiety has a unique electronic factor and is utilized as an excellent acceptor for fluorescent D–π–A small organic molecules. Replacement of C_2H_2 in the terminal phenyl group of α-cyanostilbene with a sulfur atom enhances the luminescence properties of donor–π–acceptor systems. Thus, such potent acceptors can display a significant interaction with 1,4,5-triphenyl imidazole through the vinylbenzene π-linker with good ICT properties. All dyes showed good solvatochromic properties. **2b**, **2c**, and **2d** dyes showed great AIE behavior with noticeable MFC properties (Scheme 1).

2. Result and discussion

2.1. Synthesis and characterization

The dyes were synthesized as depicted in Scheme 2. Thus, one-pot three components condensation reaction of equimolar quantities of benzil, terephthalaldehyde, and aniline in the presence of ammonium acetate and glacial acetic acid afforded the corresponding imidazole product 1 that underwent Knoevenagel condensation reaction with different acceptors using 5% NaOH or sodium acetate anhydrous (at room-temperature for **2a**, 100 °C for **2b** and 80 °C for **2c** and **2d**) to afford the **2a–2d** dyes in good yield. All compounds were confirmed with the conventional spectroscopic tools. The ESI† contains the NMR, the attenuated total reflectance–Fourier transform infrared (ATR–FTIR) and high-resolution mass spectrometry (HRMS) charts for the synthesized compounds.

2.2. Optical properties

Imidazole-based D–π–A dyes **2a–2d** have ICT character because they contain 1,4,5-triphenyl-1*H*-imidazole moiety as the electron donor (D) and 1-indanone, 1,3-indandione, 2-phenylacetonitrile, and 2-thiopheneacetonitrile as electron acceptors (A). Accordingly, different solvents of varying polarity were used to study the solvatochromic effect in both UV-Vis absorption and fluorescence spectra. The values of the maximum absorption wavelength (λ_{max}), molar extinction coefficients (ε), and Stokes Shifts are presented in Table 1. The dyes **2a–2d** displayed two main absorption bands at 230, 376 nm, 231, 437 nm, 230, 368 nm, and 230, 375 nm, respectively. The first absorption band is usually assigned to the π–π* transition in a short-wavelength region, and the second band is due to ICT band at a long wavelength region.[60] Noticeably, the red shift in λ_{max} of the four dyes and the differences in the molar extinction coefficient values indicate the presence of ICT in the dyes.[61,62] Fig. 1 shows a comparative UV-Vis absorption and fluorescence of **2a–2d** dyes in DCM solution. The ICT band is red-shifted in accordance with the electron affinity difference among the acceptors used. It is known that a higher electron affinity acceptor in D–π–A system increases the ICT character and thus lower the energy gap between the excited state and the ground state.[32] On the other hand, dyes **2a–2d** exhibited emission λ_{max} in DCM solution at 528, 574, 493 and 505 nm with 0.71, 0.05, 0.14 and 0.16 relative fluorescence quantum yields, respectively. The Stokes shifts of dyes **2a–2d** were calculated to be 7656, 5462, 6890, and 7080 cm^{-1}, respectively. The observed high Stokes

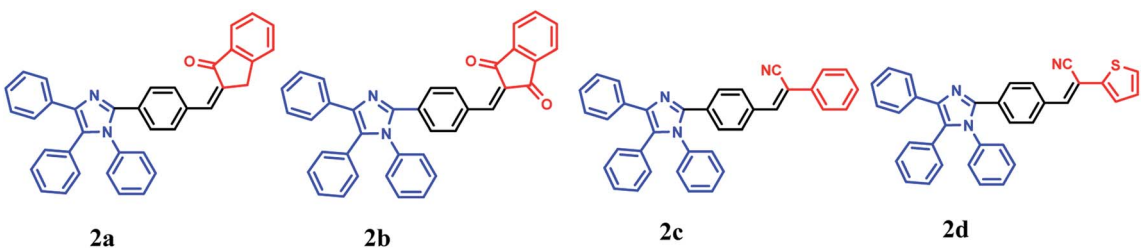

Scheme 1 The molecular structure of dyes **2a–2d**.

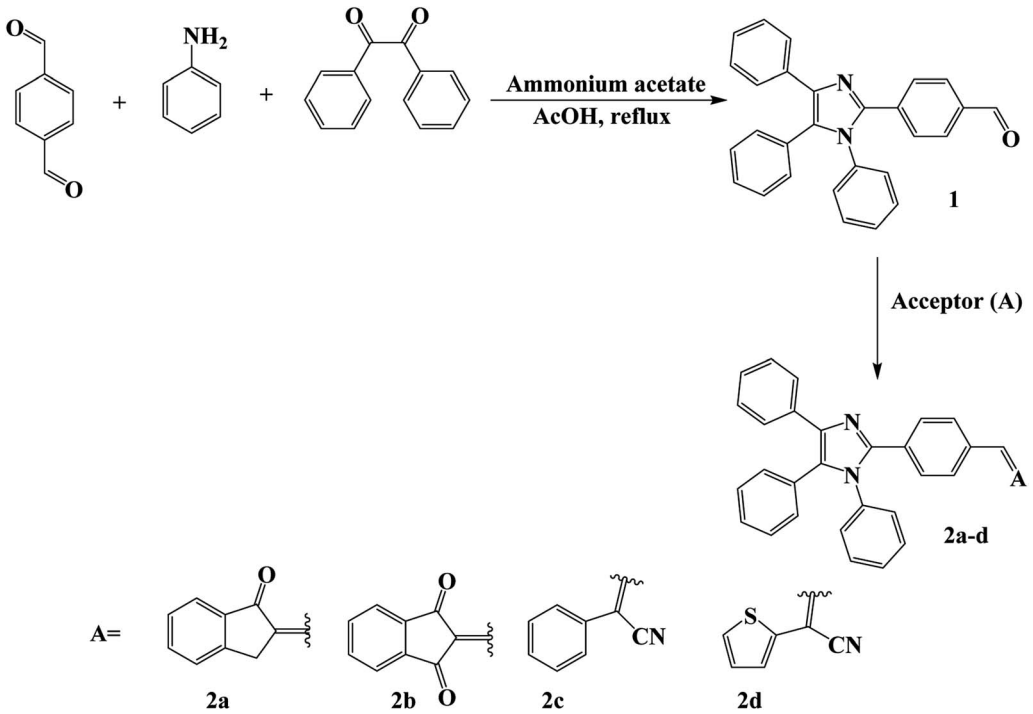

Scheme 2 Synthesis of **2a–2d** dyes.

shift values for the dyes may improve charge transfer at the molecules' locally excited state.[57] The results of emission indicate that the emission intensity of these dyes was dependent on the dye structure to reveal that dye **2a** was the highest in both fluorescence intensity and the Stokes shift, even in comparison to tetraphenyl imidazole compound TIBM, which has a Stokes

Table 1 Summary of the optical data for dyes **2a–2d** in different solvents

Dye	Solvent	Solvent polarity $E_T(30)^a$, (kcal mol^{-1})	Absorption wavelength λ_{max} (nm)	Molar extinction coefficient ε (M^{-1} cm^{-1})	Excitation wavelength λ_{ex}	Emission wavelength λ_{em} (nm)	$\Phi_f{}^b$	Stokes Shift $(\Delta\nu)^c$ (cm^{-1})
2a	Hexane	31.0	379	2.0×10^4	384	426	0.71	4114
	Toluene	33.9	382	2.8×10^4	387	466		4719
	EtAc	38.1	376	2.9×10^4	381	498		6515
	DCM	40.7	376	3.0×10^4	381	528		7656
	Acetone	42.2	374	3.0×10^4	379	534		8011
	MeCN	45.6	372	2.4×10^4	377	550		8700
2b	Hexane	31.0	432	1.1×10^4	437	476	0.05	2140
	Toluene	33.9	442	2.9×10^4	447	526		3613
	EtAc	38.1	432	2.7×10^4	437	562		5355
	DCM	40.7	437	2.8×10^4	442	574		5462
	Acetone	42.2	424	2.9×10^4	429	592		6693
	MeCN	45.6	422	2.4×10^4	427	599		7002
2c	Hexane	31.0	367	7.3×10^3	372	453	0.14	4417
	Toluene	33.9	377	4.0×10^4	382	463		4927
	EtAc	38.1	370	4.6×10^4	375	491		6660
	DCM	40.7	368	3.8×10^4	373	493		6890
	Acetone	42.2	363	4.1×10^4	368	510		7940
	MeCN	45.6	369	4.2×10^4	374	520		7870
2d	Hexane	31.0	370	0.1×10^2	375	439	0.16	4248
	Toluene	33.9	389	2.8×10^4	394	466		4248
	EtAc	38.1	374	3.0×10^4	379	494		6495
	DCM	40.7	375	2.6×10^4	380	505		6865
	Acetone	42.2	377	3.5×10^4	382	517		7183
	MeCN	45.6	379	4.1×10^4	384	529		7482

[a] Empirical parameters of solvent polarity $E_T(30)$.[61] [b] The relative fluorescence quantum yields of **2a–2d** solutions in DCM using rhodamine solution in EtOH ($\phi = 0.94$) as a standard.[64] [c] Stokes shift was estimated using the equation of $(\Delta\nu) = 10\ 7\ (1/\lambda_{em}) - (1/\lambda_{ab})$.

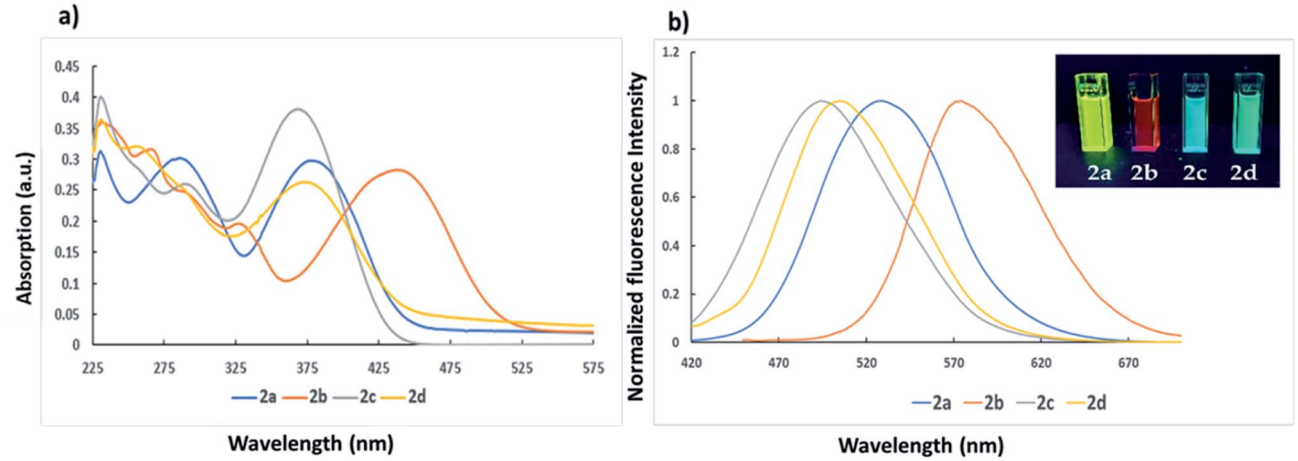

Fig. 1 (a) Absorption and (b) normalized emission of dyes **2a–2d** solution in DCM (1×10^{-5} M) at RT.

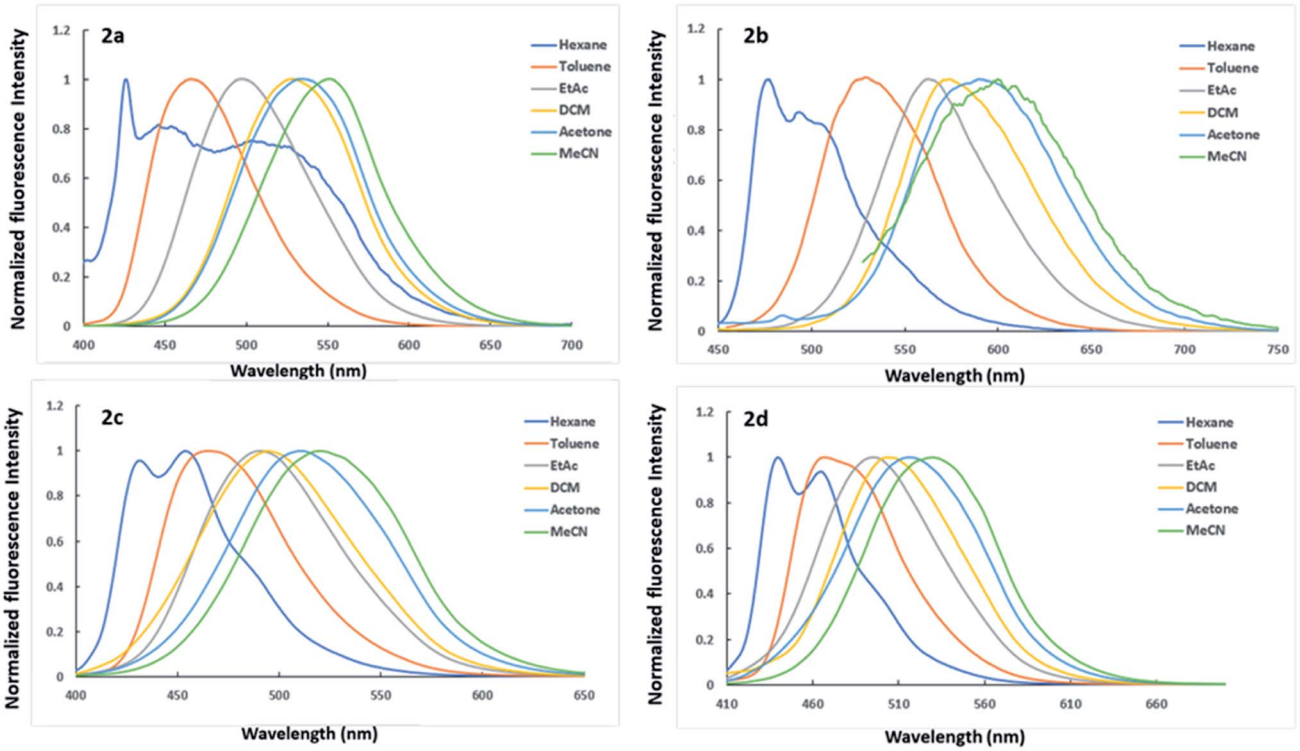

Fig. 2 Normalized emission of dyes **2a–2d** solution in different solvents (1×10^{-5} M) at RT.

shift value of 6327 (ref. 59) (Fig. 1 and Table 1). Implying that the chemical structure difference may affect the ICT state's relative proximity with the low-lying triplet and/or ground states, and the intramolecular relaxation may be complete for dye **2a** compared with other dyes, respectively. The observed high molar extinction coefficients for the dyes (Table 1) indicate their suitability for optoelectronic applications.[63] The results of solvatochromism are summarized in Table 1 and shown in Fig. S1† (absorption) and Fig. 2 (emission).

As shown in Fig. 2, the solvents with a higher polarity have a better chance of stabilizing excited states than those with a lower polarity. The solvatochromic features of dyes should be attributed to the fact that solvent molecules with high polarity efficiently reduce the energies of excited states and enhance the ICT effect, resulting in a red shift of the fluorescence. In comparison to the emission spectra (Fig. 2), the absorption spectra of dyes (Fig. S1†) are even less sensitive to changes in solvent polarity showed weak solvatochromism to indicate that the ground states are less polar than the excited states.[10,65,66]

Furthermore, the correlation of solvent polarity $E_T(30)$ and the wavenumber of absorption, fluorescence lambda maxima, and the Stokes shifts of the dyes **2a–2c** are shown in Fig. 3. As

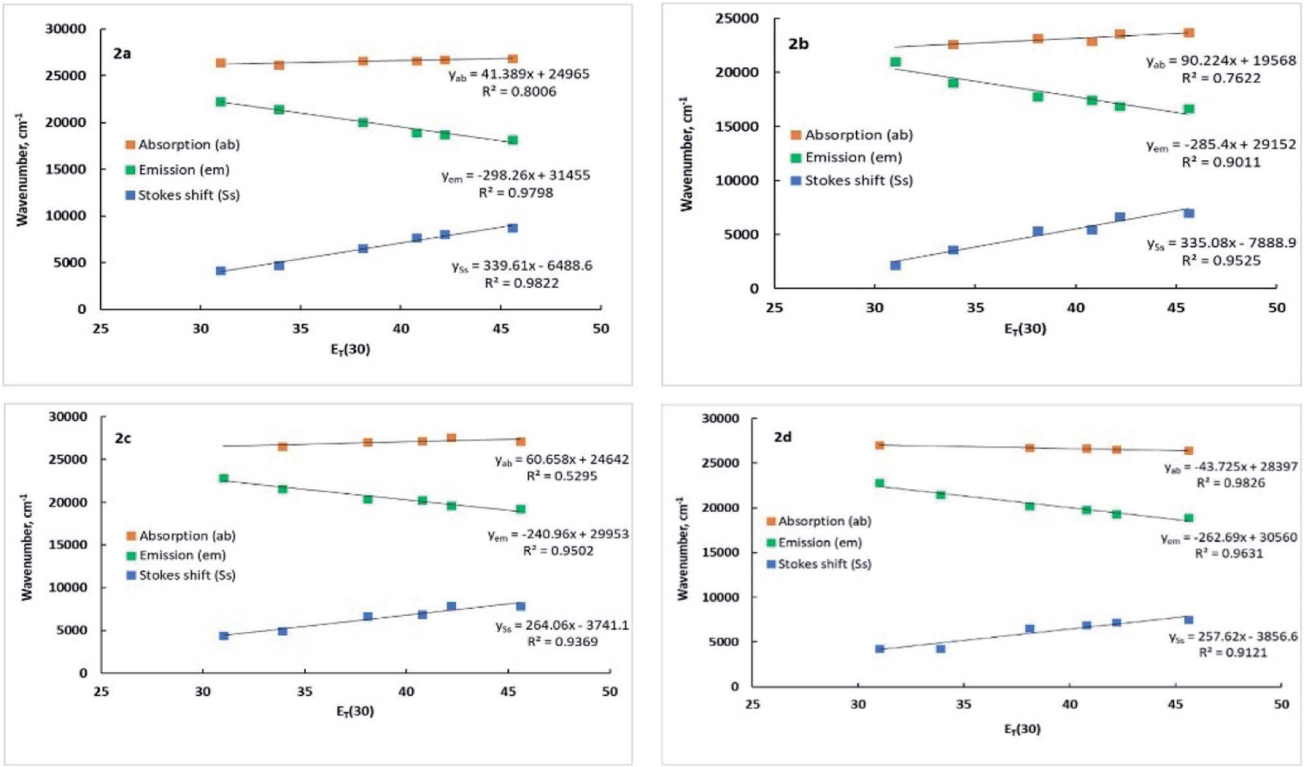

Fig. 3 The Stokes shift, the absorption, and fluorescence maximum wavenumber of dyes **2a–2d** *versus* the solvent polarity ET(30) of different solvents.

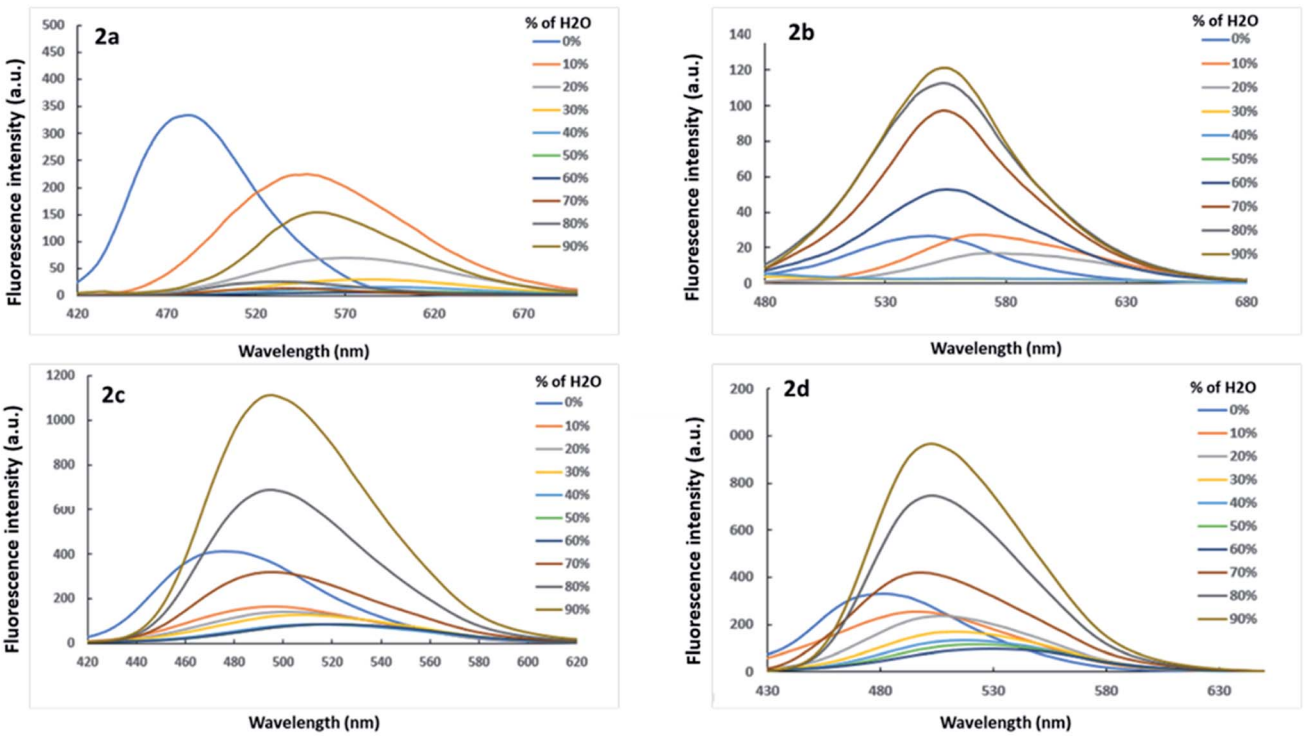

Fig. 4 Emission of dyes **2a–2d** in dioxane–water mixtures with different water volume fractions (1×10^{-5} M) at RT. Excitation wavelengths depend on λ_{max} of each dioxane–water mixture as shown in the supporting information† (Fig. S1†).

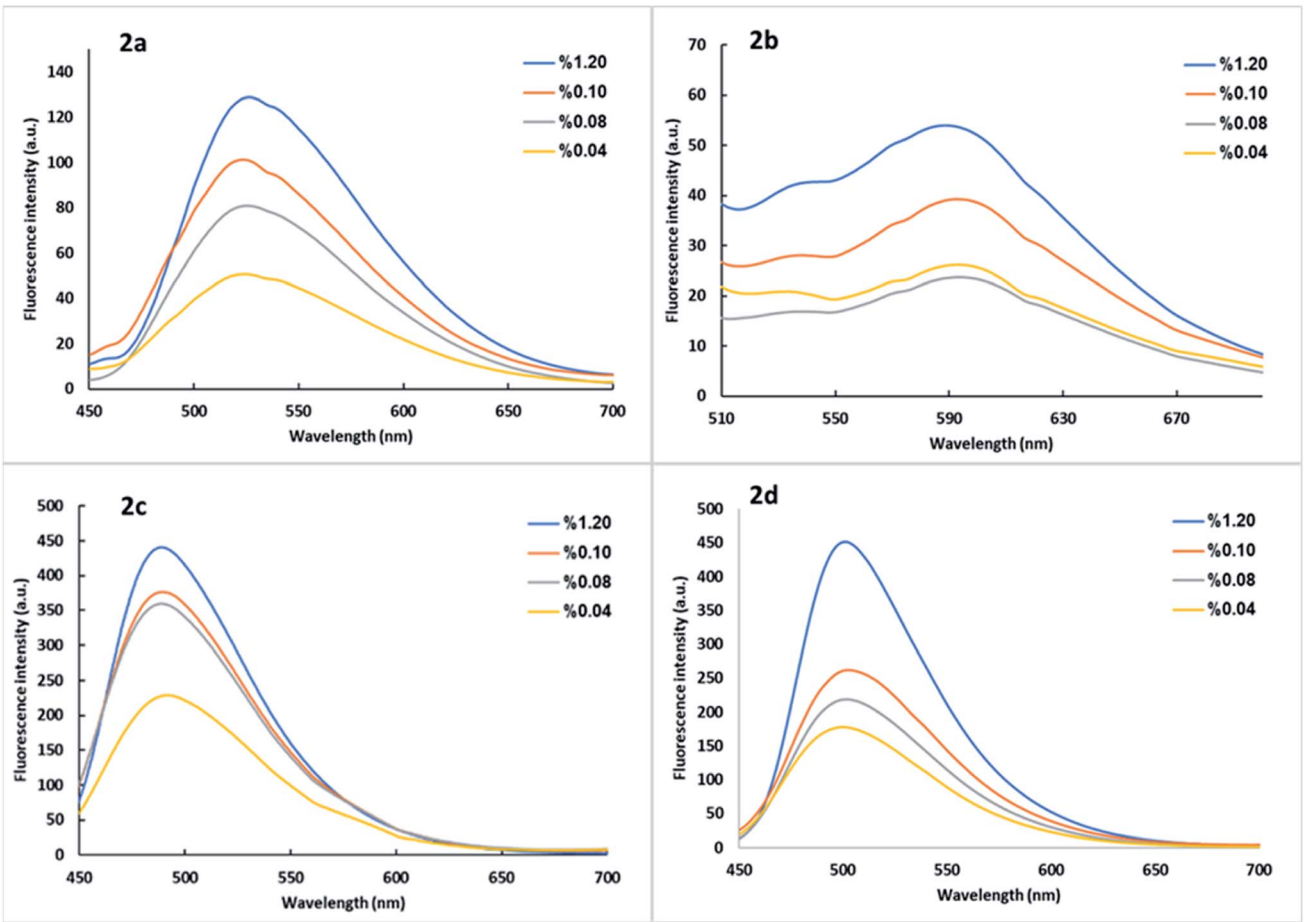

Fig. 5 Steady-state fluorescence of dyes **2a–2d** using NaCl as a diluent at selected excitation wavelengths of the dye in DCM solution 1×10^{-5} M (Table 1).

shown in Fig. 3, the dyes **2a–2c** exhibited a red shift in fluorescence and a slight blue shift in the absorption spectra upon increasing the solvent polarity, implying that the excited states are more polar than the ground states. The slope of increasing the Stokes shift as the polarity of the solvent increases was in the order **2a** > **2b** > **2c**. These results indicate that the stabilization of the intramolecular relaxation of the ICT was much enhanced for **2a**, followed by **2b** and **2c**. Dye **2d**, on the other hand, revealed a slight red shift in the absorption spectra but far lower than the red shift observed for the fluorescence spectra upon increasing the polarity of the solvent and showing a similar manner to dyes **2a–2c** as the Stokes shift was proportional to the solvent polarity. The Stokes shift is very much affected by the microenvironment around the fluorophore. Thus typical D–π–A fluorophore would respond to the polarity changes due to the interaction of ICT and the polarity of the medium. Therefore, the observed large Stokes shift would be attributed to the structural relaxation and stabilization of the excited states, which was assisted by large solvent polarity. Similar behavior of D–π–A system in different solvents was recently reported.[35]

2.3. Aggregation-induced emission

The aggregation-induced emission (AIE) behavior of the dyes was investigated by tracking the changes of fluorescent intensity in water ratio in dioxane–water solvent mixture, where dioxane acts as a good solvent and water acts as a non-solvent (Fig. 4). When the addition of water is ≤60%, it decreases the emission intensity of dyes due to aggregation caused quenching. On the other hand, in increments of water ratio ≥60%, an AIE appears at a longer wavelength, revealing an increase in the emission intensity again. This result is attributed to restricted intramolecular rotations and rigid molecular conformations.[67] Among all dyes, dye **2a** showed weak AIE behavior, and thus it is expected to show weak MFC properties. The presence of sp^3 carbon in the acceptor moiety present in dye **2a** rendered it certain geometry that did not promote AIE compared with dyes **2b–2d**.

The two extremes shown for the optical properties of the dyes in pure dioxane and 90% water–dioxane mixture reveal interesting results (Fig. S2, S3† and Fig. 4). It is indicated in these figures that the absorption of the dyes in the 90% water–dioxane mixture showed slight and irregular shifts of the wavelengths compared with those in pure dioxane. However, the fluorescence

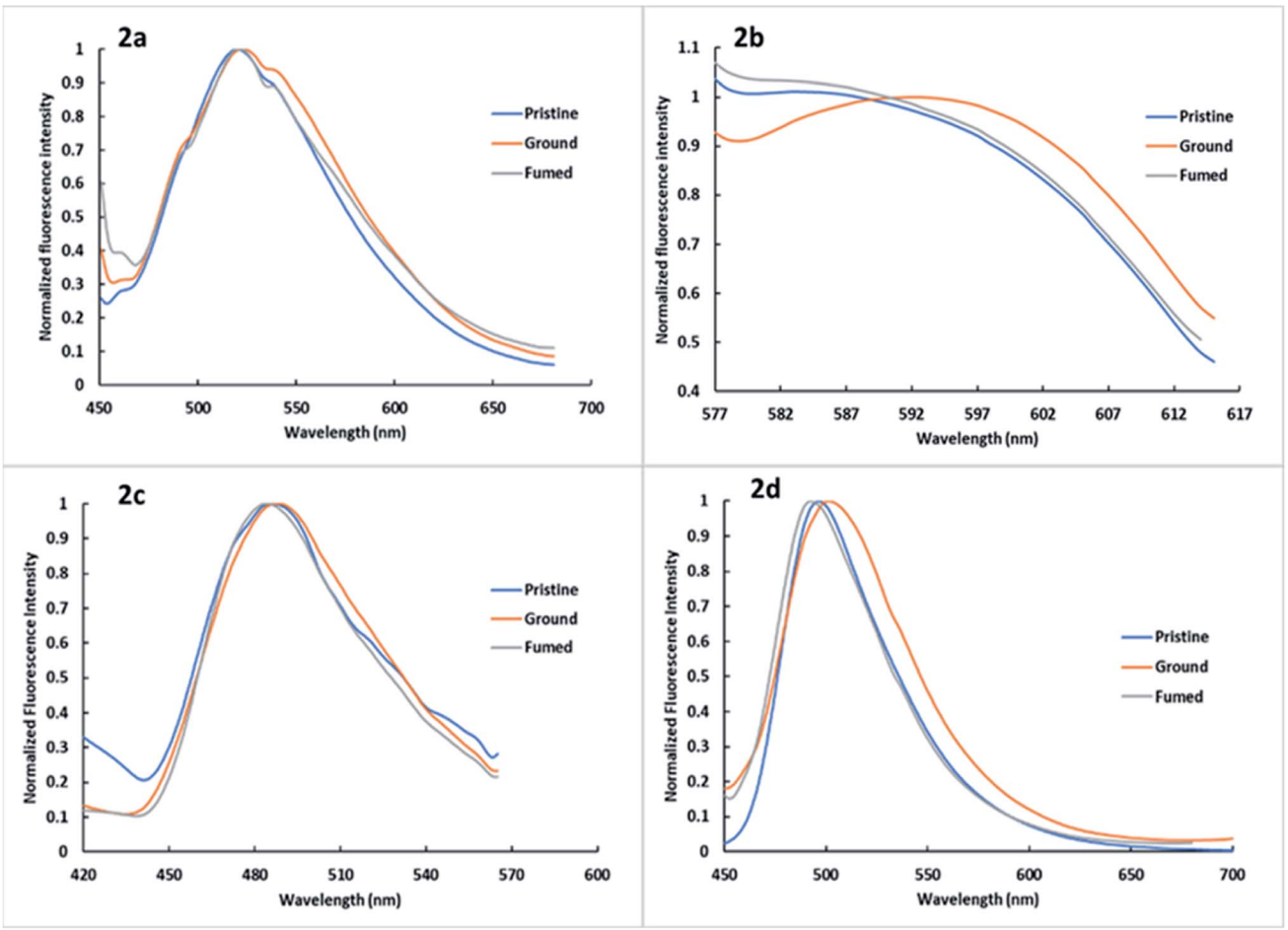

Fig. 6 Solid state fluorescence of **2a–2d** pristine, ground and fumed at selected excitation wavelengths of the dye in DCM solution 1×10^{-5} M (Table 1).

Table 2 Summary of the emission wavelength λ_{em} for dyes **2a–2d** in the solid state

	Emission wavelength λ_{em} (nm)		
Dye	Pristine	Ground	Fumed
2a	520	522	521
2b	583	592	586
2c	486	488	484
2d	495	501	493

of the dyes in the 90% water–dioxane mixture showed clear redshifts of the wavelengths compared with those in pure dioxane. This result indicates that the excited states are more polar than the ground states in similar behaviour to the results of the solvent effect presented above. As explained for the solvent effect above, the high polarity of the 90% water–dioxane mixture was favourable for both ICT stabilization and the AIE effect.[68]

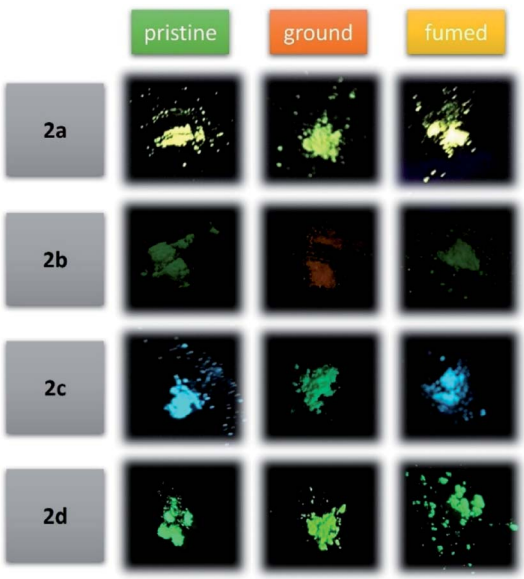

Fig. 7 Fluorescence photographs of colour changes of **2a–2d** pristine, ground and fumed.

2.4. Solid state fluorescence

One easy way to reveal the emission of the solid-state dyes, an optically transparent solid such as NaCl was used as a diluent for

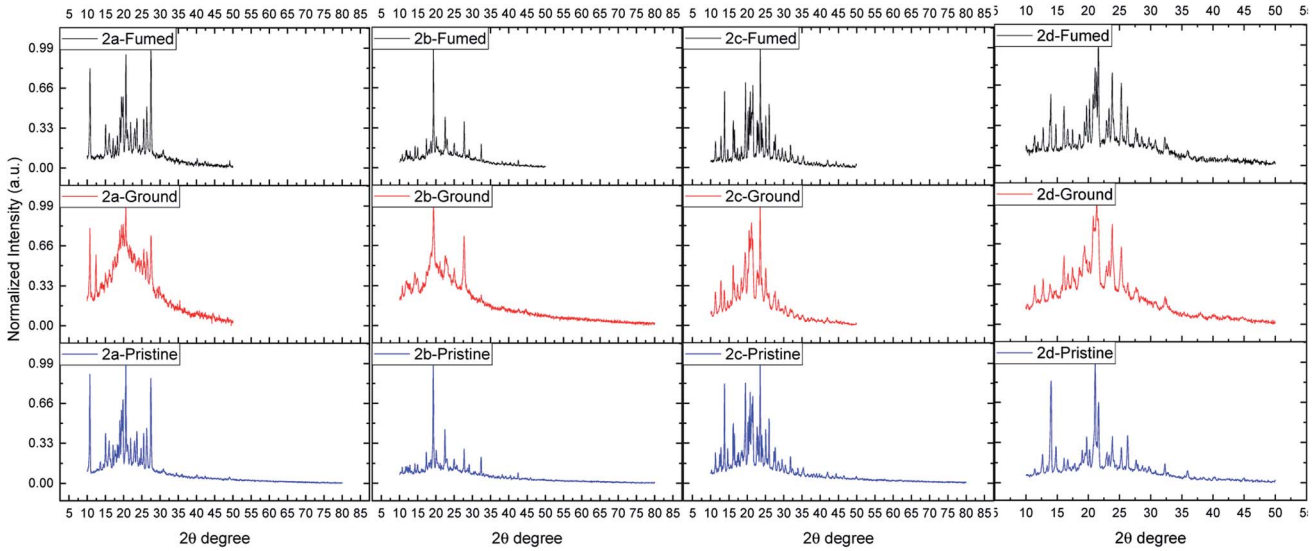

Fig. 8 Normalized XRD patterns of pristine, ground, and fumed of dyes **2a–2d**.

the dye, and 1 mm quartz cell was used for the solid mixture measurement. Likewise, in the thin film case,[69] the solid mixtures were placed in the quartz cell that was held in the cell holder in a diagonal position, and the fluorescence was measured at selected excitation wavelengths of the dye in DCM solution (see Table 1). Fig. 5 shows steady-state fluorescence spectra of the dye **2a–2d** as a function of the dye content in NaCl. A positive correlation between solid-state fluorescence intensity and the solid mixture's dye content indicates the AIE of all dyes.

2.5. Mechanofluorochromic (MFC) properties

To gain a better understanding of the MFC properties, the solid-state of dyes (pristine, ground, and fumed) was examined by solid-state fluorescence spectroscopy (Fig. 6 and Table 2), fluorescence photography (Fig. 7), powder X-ray diffraction (XRD) (Fig. 8) and scanning electron microscopy (SEM) (Fig. 9).

Based on their AIE properties, the mechanochromic properties of **2a–2d** were explored. As shown in Fig. 6, 7 and Table 2. In the pristine form, **2a** showed yellow emission, **2b** showed green emission, while **2c** exhibited blue emission, and **2d** showed green emission with the emission values of 520, 583, 486, and 495 nm, respectively. Upon grinding using a mortar and pestle, the pristine crystals of **2a–2d** converted to pale-green, orange, parakeet-green and green fluorescence and the emission peaks red-shifted to 521, 586, 484 and 493 nm, respectively. When the ground powder was fumed, the fluorescence emissions of the ground powders were restored to their original state. The MCF observed indicates that grinding the dyes causes conformational changes and phase transition from crystalline to relatively amorphous in the molecules in such a way to be more coplanar and thus enhancing the ICT delocalization leading to emission at a longer wavelength.[70]

The XRD curves of all the dyes in pristine state displayed sharp diffraction peaks, indicating that they were in an ordered arrangement of crystalline states. After grinding, the samples exhibited broad peaks. This means that the order of the molecules has altered from a crystalline to an amorphous structure or disorganized molecule packing. After fuming the samples with ethanol for 5 minutes, then air-drying, sharp peaks restored.[71] These findings suggest that the four compounds have reasonably good MCF characteristics. The transition between the ordered crystalline and disordered amorphous phases is the primary cause of the MFC behaviors mechanism.[72]

The same suggestion will apply to SEM images. From SEM images, the compounds **2b**, **2c** and **2d** in the pristine state show crystalline phase wherein the ground states we noticed that the crystalline shape is destroyed and form amorphous phase. After fuming, the samples recovered and showed a crystalline phase. For **2a**, we observed the crystalline phase in a pristine state, and after grinding, we got an amorphous phase, but in the fuming state, it showed a different manner. It is noticed that the crystalline and amorphous phase gives a weak MFC behavior among the dyes, which we expected previously.

2.6. Theoretical calculations

The characterization of the optical and electronic properties of the dyes is beneficial to analyze their HOMOs, LUMOs and band gaps. Knowing the HOMO and LUMO orbitals' relative ordering indicates the excitation properties.[73] All calculations were performed by the Gaussian 09 program. Density functional theory (DFT) with B3LYP[30] functional at the 6-31G(d) basis set was used to optimize the ground-state geometries of dyes **2a–2d** and ground-state structure and energy levels were obtained under the same framework. Time-dependent DFT (TD-DFT) with the B3LYP and the 6-31G(d) basis set were used to acquire the corresponding absorption and fluorescence spectrum.

Based on the results shown in Fig. 10 and Table 3, the HOMO of dyes is distributed on the donor unit, while the LUMO is mostly placed on the acceptor unit. This reveals that the HOMO–LUMO transition has a great ICT character. The energy

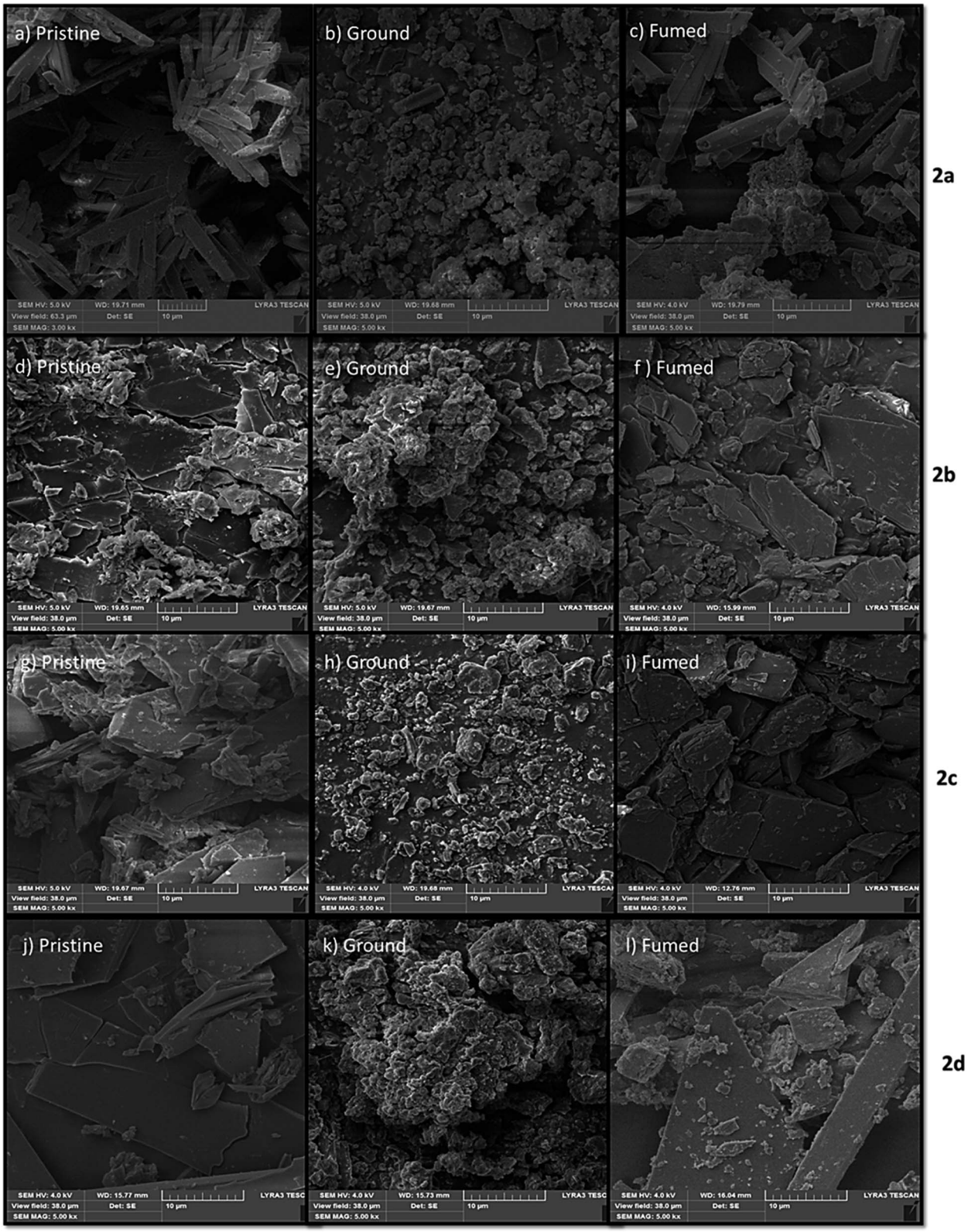

Fig. 9 SEM micrographs of pristine, ground, and fumed of dyes **2a–2d**.

gaps of **2a–2d** dyes are 3.18, 2.92, 3.20 and 3.05 eV, respectively. The dyes showed HOMO level at −5.56, −5.67, −5.48, −5.43 eV, respectively. Moreover, their LUMO levels are in the range of −2.38, −2.75, −2.28 and −2.38 eV. The computed energy gaps of the dyes nicely reflect the experimental absorption lambda max difference among the dyes.

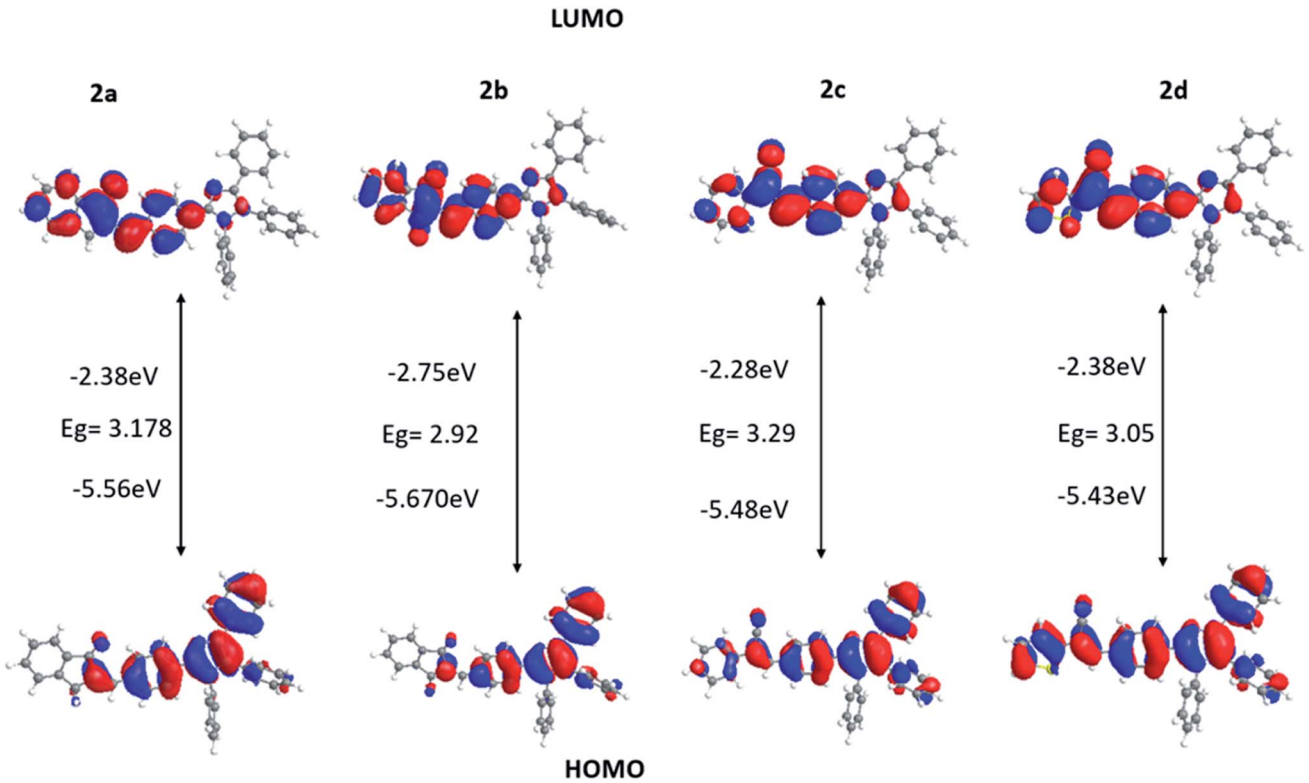

Fig. 10 The energies and electron density distribution of HOMO and LUMO orbitals of dyes **2a–2d**.

Table 3 Theoretical band gaps of **2a–2d**

				HOMO[b]			LUMO[b]		
Dyes	E^{HOMO}[a] [eV]	E^{LUMO}[a] [eV]	E_g[a] (eV)	Donor	π-spacer	Acceptor	Donor	π-spacer	Acceptor
2a	−5.56	−2.38	3.18	72	19	9	6	28	74
2b	−5.67	−2.75	2.92	78	15	7	7	25	68
2c	−5.48	−2.28	3.30	73	16	11	9	32	59
2d	−5.43	−2.38	3.05	62	17	21	8	29	63

[a] The calculated HOMOs, LUMOs, and band gaps [E^{LOMO}–E^{HOMO}] were made at TD-DFT/B3LYP. [b] The Molecular orbital contributions based on Mulliken type.

3. Experimental

3.1. Materials and instruments

Solvents and reagents with high pureness were purchased from Sigma Aldrich firm. Using a Bruker Avance 600 and 850 MHz spectrometers for analyzing ^{1}H and ^{13}C NMR spectra that were reported in a solution of $CDCl_3$-d_1. On PerkinElmer spectra 100 FTIR spectrometer, Infrared spectra were obtained. Determination UV absorption spectra in dichloromethane by Shimadzu UV-Vis Spectrophotometer. Recording Fluorescence spectra by PerkinElmer LS 55 Fluorescence Spectrometer. In open capillary tubes melting points have been determined by a Stuart Scientific melting point apparatus. Morphological properties of the dyes were examined by Field emission scanning electron microscopy FESEM using (Jeol JSM-7600F) Quanta instrument. And for X-ray diffraction analysis were recorded on X-ray Diffractometer model type (RIGAKU ULTIMA-IV) (Mannai Technical Services), and Ni-filtered CuKa radiations at 40 kV voltages and 40 mA over a scanning range between 10° and 60°. High-resolution mass spectra were obtained using OrbitrapID-X spectrometer (FTMS + p ESI).

3.2. Synthesis of 4-(1,4,5-triphenyl-1*H*-imidazole-2-yl) benzaldehyde (1)

Terephthalaldehyde (1.34 g, 10.00 mmol) and aniline (0.93 g, 10.00 mmol) were dissolved in acetic acid (100 mL) and stirred for 1 h at room temperature. Benzil (2.10 g, 10.00 mmol) and ammonium acetate (5.39 g, 70.00 mmol) were added subsequently. The mixture was heated at 120 °C overnight. After termination of the reaction, the solution was poured into copious amounts of water. After neutralization, the solid was collected by filtration and washed with water. Silica gel column

purification with ethyl acetate: petroleum ether (1 : 9) gave a light-yellow crystal of 1 (1.60 g, yield = 40%), m.p. 183 °C.[59]

^{1}H NMR (850 MHz, $CDCl_3$) δ: 9.99 (s, 1H, aldehyde C=O), 7.78 (d, 2H, J = 8.07 Hz, Ar–H), 7.66 (d, 2H, J = 8.12 Hz, Ar–H) 7.64 (d, 2H, J = 7.84 Hz, Ar–H), 7.37 (t, 1H, J = 7.31 Hz, Ar–H), 7.33 (t, 2H, J = 7.63 Hz, Ar–H), 7.30 (t, 2H, J = 7.56 Hz, Ar–H), 7.24–7.28 (m, 4H, Ar–H), 7.16 (d, 2H, J = 7.83 Hz, Ar–H),7.10 (d, 2H, J = 7.86 Hz, Ar–H).

^{13}C NMR (213 MHz, $CDCl_3$) δ: 191.84, 145.27, 138.88, 138.65, 136.63, 135.74, 135.47, 133.49, 132.11, 131.17, 129.93, 129.77, 129.60, 129.56, 129.37, 129.04, 128.62, 128.54, 128.42, 128, 40, 127.59, 127.25, 120.06.

IR (cm^{-1}): C–H aromatic 3052, C=O aldehyde 1698, C=C stretch 1602.

3.3. Synthesis of (*Z*)-2-(4-(1,4,5-triphenyl-1*H*-imidazole-2-yl) benzylidene)-2,3-dihydro-1*H*-inden-1-one (2a)

To a solution of **1** (0.40 g, 1.00 mmol) and 1-indanone (0.26 g, 2.00 mmol) in ethanol (10 mL) was added, 5 mL of solution of sodium hydroxide 5%. The solution was further stirred at room temperature for 3–5 h to afford a yellow precipitate, which were filtered off, and neutralized by 1 M HCL. Then washed several times with water. Silica gel column purification with dichloromethane gave a yellow powder of **2a** (0.41 g, yield = 80%), m.p. 280 °C.

^{1}H NMR (600 MHz, $CDCl_3$) δ: 7.90 (d, 1H, J = 7.60 Hz, Ar–H), 7.60–7.63 (m, 4H, Ar–H), 7.54–7.56 (m, 6H, Ar–H), 7.452 (t, 1H, J = 7.38 Hz, Ar–H), 7.30–7.36 (m, 2H, Ar–H), 7.27–7.28 (m, 2H, Ar–H), 7.21–7.25 (m, 4H, Ar–H), 7.14 (d, 2H, J = 8.23 Hz, Ar–H), 7.10 (d, 2H, J = 8.33 Hz, Ar–H), 4.03 (s, 2H, CH_2).

^{13}C NMR (150 MHz, $CDCl_3$) δ: 194.37, 149.70, 145.63, 138.02, 134.90, 133.07, 131.62, 131.21, 131.17, 130.68, 129.64, 129.20, 128.69, 128.62, 128.49, 128.42, 127.87, 127.57, 126.34, 124.61 32.66.

IR (cm^{-1}): C–H aromatic 3061, C=O ketone 1686, C=C stretch 1601.

HRMS (ESI): m/z calcd for $C_{37}H_{27}N_2O$ 515.2123 $[M + H]^+$, found 515.2118.

3.4. Synthesis of 2-(4-(1,4,5-triphenyl-1*H*-imidazole-2-yl) benzylidene)-1*H*-indene-1,3(2*H*)-dione (2b)

To a solution of **1** (0.40 g, 1.00 mmol) and 1,2-indanedione (0.15 g, 1.00 mmol) in ethanol (10 mL) sodium acetate anhydrous (0.40 g, 5.00 mmol) was added. The mixture was heated overnight at 100 °C to afford a yellow precipitate After termination of the reaction, the solution was poured into copious amounts of water. After neutralization, the solid product was collected by filtration and washed with water. Silica gel column purification with dichloromethane gave a yellow powder of **2b** (0.39 g, yield = 75%), m.p. 260 °C.

^{1}H NMR (850 MHz, $CDCl_3$) δ: 8.39 (d, 2H, J = 8.42 Hz, Ar–H), 7.99–8.01 (m, 2H, Ar–H), 7.84 (s, 1H, aliphatic C=CH), 7.81–7.82 (m, 2H, Ar–H), 7.62 (d, 4H J = 6.89 Hz, Ar–H), 7.37 (t, 1H, J = 7.38 Hz, Ar–H), 7.33 (t, 2H, J = 7.61 Hz, Ar–H), 7.28 (t, 2H, J = 7.44 Hz, Ar–H), 7.22–7.26 (m, 4H, Ar–H), 7.14 (d, 2H, J = 6.97 Hz, Ar–H), 7.11 (d, 2H, J = 7.14 Hz, Ar–H).

^{13}C NMR (213 MHz, $CDCl_3$) δ: 190.17, 189.12, 146.01, 145.39, 145.04, 142.50, 140.05, 135.44, 135.27, 134.15, 133.45, 132.08, 131.06, 129.47, 129.24, 129.11, 128.93, 128.80, 128.55, 128.53, 128.47, 128.29, 127.49, 127.10, 125.08, 123.34, 123.31, 119.91.

IR (cm^{-1}): C–H aromatic 3057, C=O ketone 1723, 1685, C=C stretch 1588.

HRMS (ESI): m/z calcd for $C_{37}H_{25}N_2O_2$ 529.1916 $[M + H]^+$, found 529.1911.

3.5. Synthesis of (*Z*)-2-(4-(2-isocyano-2-phenylvinyl)phenyl)-1,4,5-triphenyl-1*H*-imidazole (2c)

To a solution of **1** (0.40 g, 1.00 mmol) and phenylacetonitrile (0.12 g, 1.00 mmol) in ethanol (10 mL) was added, 5 mL of solution of sodium hydroxide 5%. The mixture was heated at 80 °C for 2–3 h to afford yellow precipitate, which were filtered off, and neutralized by 1 M HCL. Then washed several times with water and wash once by ethanol to obtain a yellow product **2c** (0.42 g, yield = 84%), m.p. 240 °C.

^{1}H NMR (600 MHz, $CDCl_3$) δ: 7.79 (d, 2H, J = 8.45 Hz, Ar–H), 7.66 (d, 2H, J = 7.24 Hz, Ar–H), 7.61 (d, 2H, J = 7.12 Hz, Ar–H), 7.56 (d, 2H, J = 8.50 Hz, Ar–H),7.47 (s, 1H, aliphatic C=CH), 7.43–7.45 (m, 2H, Ar–H), 7.30–7.41 (m, 4H, Ar–H), 7.27–7.28 (m, 2H, Ar–H), 7.20–7.25 (m, 4H, Ar–H), 7.14 (dd, 2H, J = 8.07, 1.47 Hz, Ar–H), 7.10 (dd, 2H, J = 8.19, 1.29 Hz, Ar–H).

^{13}C NMR (150 MHz, $CDCl_3$) δ: 145.65, 141.45, 134.58, 131.79, 131.25, 129.58, 129.45, 129.38, 129.31, 129.24, 128.62, 128.47, 128.42, 127.70, 126.16, 118.06, 111.95.

IR (cm^{-1}): C–H aromatic 3051, C≡N 2210, C=C stretch 1595.

HRMS (ESI): m/z calcd for $C_{36}H_{26}N_3$ 500.2127 $[M + H]^+$, found 500.2121.

3.6. Synthesis of (*Z*)-2-(4-(2-isocyano-2-(thiophen-2-yl)vinyl) phenyl)-1,4,5-triphenyl-1*H*-imidazole (2d)

To a solution of **1** (0.40 g, 1.00 mmol) and 2-thiopheneacetonitrile (0.13 g, 1.00 mmol) in ethanol (10 mL) was added, 5mL of solution of sodium hydroxide 5%. The mixture was heated at 80 °C for 2–3 h to afford yellow precipitate, which were filtered off, and neutralized with water. Then washed several times with water and wash once by ethanol to obtain a yellow product **2d** (0.41 g, yield = 82%), m.p. 249 °C.

^{1}H NMR (600 MHz, $CDCl_3$) δ: 7.75 (d, 2H, J = 8.48 Hz, Ar–H), 7.62 (d, 2H, J = 7.16 Hz, Ar–H), 7.55 (d, 2H, J = 8.49 Hz, Ar–H), 7.37 (dd, 2H, J = 3.66, 1.02 Hz, Ar–H), 7.30–7.36 (m, 5H, Ar–H), 7.27–7.28 (m, 2H, Ar–H), 7.20–7.25 (m, 4H, Ar–H), 7.15 (dd, 2H, J = 7.92, 1.26 Hz, Ar–H), 7.09 (dd, 2H, J = 7.92, 1 Hz, Ar–H), 7.07 (dd, 2H, J = 5.07, 3.70 Hz, Ar–H).

^{13}C NMR (150 MHz, $CDCl_3$) δ: 145.68, 142.47, 139.37, 138.80, 138.42, 136.78, 133.30, 131.81, 131.64, 131.24, 131.22, 130.13, 130.08, 129.55, 129.42, 129.31, 129.24, 129.10, 129.04, 128.84, 128.59, 128.47, 128.44, 128.40, 128.30, 127.64, 127.60, 127.53, 127.33, 127.17, 126.57, 119.08, 116.89, 106.30.

IR (cm^{-1}): C–H aromatic 3054, C≡N 2214, C=C stretch 1595.

HRMS (ESI): m/z calcd for $C_{34}H_{24}N_3S$ 506.1691 $[M + H]^+$, found 506.168.

3.7. Computational methodology

The optimization of the ground state of the compounds was made by Gaussian 09 program, the density functional theory (DFT), and the linear-response time-dependent density functional theory (TD-DFT).[74,75] Calculating energy gaps and frontier molecular orbitals were carried out using the Chemissian software. The vibrational frequencies calculations were undertaken to confirm that the geometry optimization corresponds to the minimum local structures. The compounds were optimized in dichloromethane in the polarizable continuum model (PCM), considering the electrostatic interactions with the solvent.[76,77] The studied compounds have been calculated with the restricted Becke, 3-parameter, Lee–Yang–Parr (B3LYP). Depending on the optimized ground state, the electronic transitions were determined at the TD-DFT approach *via* energy calculation and the oscillator strength for 50 singlet excited states.

4. Conclusion

Four new imidazole-based D–π–A dyes (**2a–2d**) have been synthesized and characterized. All dyes exhibited good emissive solvatochromism. On the other hand, **2b**, **2c**, and **2d** dyes showed an AIE activity with excellent reversible MFC properties. However, dye **2a** revealed the weakest AIE behaviour among the dyes and thus was the case was observed for its MFC property. The computed HOMO–LUMO energies, the electron density distribution of HOMO and LUMO, and the energy gaps agreed with the experimental optical data for ICT bands in all dyes and the absorption lambda max difference among the dyes. The overall results suggest that the imidazole-based D–π–A system would inspire further structural motives for possible optoelectronic applications.

Conflicts of interest

There are no conflicts to declare.

Acknowledgements

The Deanship of Scientific Research (DSR) at King Abdulaziz University (KAU), Jeddah, Saudi Arabia, has funded this project, under grant no. (KEP-PhD: 74-130-1443).

References

1 E. Horak, *et al.*, Tuneable solid-state emitters based on benzimidazole derivatives: Aggregation induced red emission and mechanochromism of D-π-a fluorophores, *Dyes Pigm.*, 2019, **162**, 688–696.
2 W. Zeng, *et al.*, Efficient non-doped fluorescent OLEDs with nearly 6% external quantum efficiency and deep-blue emission approaching the blue standard enabled by quaterphenyl-based emitters, *J. Mater. Chem. C*, 2018, **6**(16), 4479–4484.
3 S. Samanta, *et al.*, An aggregation-induced emission (AIE) active probe for multiple targets: a fluorescent sensor for Zn 2+ and Al 3+ & a colorimetric sensor for Cu 2+ and F−, *Dalton Trans.*, 2015, **44**(43), 18902–18910.
4 T. Han, *et al.*, A diethylaminophenol functionalized Schiff base: crystallization-induced emission-enhancement, switchable fluorescence and application for security printing and data storage, *J. Mater. Chem. C*, 2015, **3**(28), 7446–7454.
5 Y. Zhan, *et al.*, Phenothiazine substituted phenanthroimidazole derivatives: Synthesis, photophysical properties and efficient piezochromic luminescence, *Dyes Pigm.*, 2017, **140**, 452–459.
6 Y. Zhan, *et al.*, Reversible mechanofluorochromism and acidochromism using a cyanostyrylbenzimidazole derivative with aggregation-induced emission, *RSC Adv.*, 2017, **7**(77), 48777–48784.
7 Y. Chen, *et al.*, Quinoxaline-based cross-conjugated luminophores: charge transfer, piezofluorochromic, and sensing properties, *J. Mater. Chem. C*, 2016, **4**(36), 8496–8505.
8 W. Qiao, *et al.*, Squaraine-based AIEgens for reversible mechanochromism, sensitive and selective hypochlorite detection and photostable far-red fluorescence cell imaging, *Mater. Chem. Front.*, 2020, **4**(9), 2688–2696.
9 P. Xue, *et al.*, Recent progress in the mechanochromism of phosphorescent organic molecules and metal complexes, *J. Mater. Chem. C*, 2016, **4**(28), 6688–6706.
10 Y. Xie, *et al.*, Synthesis, crystal structures and solid-state acidochromism of multiaryl-substituted pyridine derivatives with aggregation-induced emission property, *Dyes Pigm.*, 2021, **188**, 109217.
11 Q. Li and Z. Li, Molecular packing: another key point for the performance of organic and polymeric optoelectronic materials, *Acc. Chem. Res.*, 2020, **53**(4), 962–973.
12 C. Wang and Z. Li, Molecular conformation and packing: their critical roles in the emission performance of mechanochromic fluorescence materials, *Mater. Chem. Front.*, 2017, **1**(11), 2174–2194.
13 Z. Chi, *et al.*, Recent advances in organic mechanofluorochromic materials, *Chem. Soc. Rev.*, 2012, **41**(10), 3878–3896.
14 F. Zhao, *et al.*, Aggregation-induced emission (AIE)-active highly emissive novel carbazole-based dyes with various solid-state fluorescence and reversible mechanofluorochromism characteristics, *Dyes Pigm.*, 2019, **164**, 390–397.
15 S. Pratihar, A. Bhattacharyya and E. Prasad, Achieving ACQ-AIE modulation using isostructural organic fluorophores, *J. Photochem. Photobiol., A*, 2020, **396**, 112458.
16 Y. Chen, *et al.*, Aggregation-induced emission: fundamental understanding and future developments, *Mater. Horiz.*, 2019, **6**(3), 428–433.
17 Y. Hong, J. W. Lam and B. Z. Tang, Aggregation-induced emission: phenomenon, mechanism and applications, *Chem. Commun.*, 2009, (29), 4332–4353.
18 Y. Hong, J. W. Lam and B. Z. Tang, Aggregation-induced emission, *Chem. Soc. Rev.*, 2011, **40**(11), 5361–5388.

19 J. Mei, *et al.*, Aggregation-induced emission: together we shine, united we soar!, *Chem. Rev.*, 2015, **115**(21), 11718–11940.
20 F. Arshad, A. Pal and M. P. Sk, Aggregation-Induced Emission in Carbon Dots for Potential Applications, *ECS Journal of Solid State Science and Technology*, 2021, **10**(2), 021001.
21 M. Yu, *et al.*, Promising applications of aggregation-induced emission luminogens in organic optoelectronic devices, *PhotoniX*, 2020, **1**(1), 1–33.
22 D. Ma, *Status and prospects of aggregation-induced emission materials in organic optoelectronic devices*, Aggregation-Induced Emission, 2022, pp. 171–207.
23 L. Wen, *et al.*, Engineering of aggregation-induced emission luminogens by isomeric strategy to achieve high-performance optoelectronic device, *Dyes Pigm.*, 2020, **173**, 107912.
24 Y. Yu, *et al.*, Efficient red fluorescent OLEDs based on aggregation-induced emission combined with hybridized local and charge transfer state, *Dyes Pigm.*, 2021, **184**, 108770.
25 Y.-T. Lee, *et al.*, The first aggregation-induced emission fluorophore as a solution processed host material in hybrid white organic light-emitting diodes, *J. Mater. Chem. C*, 2016, **4**(29), 7020–7025.
26 Z. Ruan, *et al.*, Novel AIE-active ratiometric fluorescent probes for mercury (II) based on the Hg 2+-promoted deprotection of thioketal, and good mechanochromic properties, *J. Mater. Chem. C*, 2018, **6**(4), 773–780.
27 K. Wang, *et al.*, Fluorescence probes based on AIE luminogen: application for sensing Hg 2+ in aqueous media and cellular imaging, *New J. Chem.*, 2018, **42**(16), 13836–13846.
28 J. Qin and Y. Tang, Application of Aggregation-Induced Emission Fluorogens for Detection and Quantification of Toxic Chemicals in Small Aquatic Organisms, in *Principles and Applications of Aggregation-Induced Emission*, Springer, 2019, pp. 317–334.
29 J. Dai, *et al.*, Aggregation-induced emission photosensitizers: from molecular design to photodynamic therapy: miniperspective, *J. Med. Chem.*, 2020, **63**(5), 1996–2012.
30 H. Gao, X. Zhao and S. Chen, AIEgen-based fluorescent nanomaterials: fabrication and biological applications, *Molecules*, 2018, **23**(2), 419.
31 X. He, *et al.*, AIE-based energy transfer systems for biosensing, imaging, and therapeutics, *TrAC, Trends Anal. Chem.*, 2020, **122**, 115743.
32 Z. Song, *et al.*, Synthesis of Imidazole-Based AIEgens with Wide Color Tunability and Exploration of their Biological Applications, *Adv. Funct. Mater.*, 2016, **26**(6), 824–832.
33 M. Danko, *et al.*, Spectral properties of Y-shaped donor-acceptor push-pull imidazole-based fluorophores: comparison between solution and polymer matrices, *J. Fluoresc.*, 2012, **22**(4), 1165–1176.
34 J. Kulhánek, *et al.*, Imidazole as a Donor/Acceptor Unit in Charge-Transfer Chromophores with Extended π-Linkers, *Chem.–Asian J.*, 2011, **6**(6), 1604–1612.
35 L. M. Nhari, *et al.*, Phenothiazine-based dyes containing imidazole with π-linkers of benzene, furan and thiophene: Synthesis, photophysical, electrochemical and computational investigation, *J. Mol. Struct.*, 2022, **1251**, 131959.
36 S. N. Al-Ghamdi, *et al.*, Advances in phenothiazine and phenoxazine-based electron donors for organic dye-sensitized solar cells, *Dyes Pigm.*, 2021, **194**, 109638.
37 R. M. El-Shishtawy, Functional dyes, and some hi-tech applications, *Int. J. Photoenergy*, 2009, **2009**, 434897.
38 M. E. Zayed, *et al.*, Experimental and theoretical study of donor-π-acceptor compounds based on malononitrile, *Chem. Cent. J.*, 2018, **12**(1), 1–10.
39 S. Sasaki, G. P. Drummen and G.-i. Konishi, Recent advances in twisted intramolecular charge transfer (TICT) fluorescence and related phenomena in materials chemistry, *J. Mater. Chem. C*, 2016, **4**(14), 2731–2743.
40 T. Matsumoto, *et al.*, Design of bond-cleavage-induced intramolecular charge transfer emission with dibenzoboroles and their application to ratiometric sensors for discriminating chain lengths of alkanes, *Mater. Chem. Front.*, 2017, **1**(11), 2368–2375.
41 R. M. El-Shishtawy, *et al.*, Synthesis of a new fluorescent cyanide chemosensor based on phenothiazine derivative, *Sens. Actuators, B*, 2017, **240**, 288–296.
42 F. A. Al-Zahrani, *et al.*, A new phenothiazine-based selective visual and fluorescent sensor for cyanide, *BMC Chem.*, 2020, **14**(1), 1–11.
43 R. Ghosh, A. Nandi and D. K. Palit, Solvent sensitive intramolecular charge transfer dynamics in the excited states of 4-N, N-dimethylamino-4′-nitrobiphenyl, *Phys. Chem. Chem. Phys.*, 2016, **18**(11), 7661–7671.
44 R. Misra, R. Sharma and S. Bhattacharyya, Exploring NLO response of 9, 10-donor-acceptor substituted Bichromophoric Anthracene Derivatives, *J. Comput. Methods Sci. Eng.*, 2010, **10**(3–6), 149–164.
45 R. M. El-Shishtawy, *et al.*, Synthesis, linear and nonlinear optical properties of a new dimethine cyanine dye derived from phenothiazine, *RSC Adv.*, 2016, **6**(94), 91546–91556.
46 R. M. El-Shishtawy, *et al.*, Thiazole azo dyes with lateral donor branch: Synthesis, structure and second order NLO properties, *Dyes Pigm.*, 2013, **96**(1), 45–51.
47 A. C. Arias, *et al.*, Materials and applications for large area electronics: solution-based approaches, *Chem. Rev.*, 2010, **110**(1), 3–24.
48 H. Sun, *et al.*, Charge-separated sensitizers with enhanced intramolecular charge transfer for dye-sensitized solar cells: Insight from structure-performance relationship, *Org. Electron.*, 2018, **61**, 35–45.
49 H. Kafafy, *et al.*, Steric and solvent effect in dye-sensitized solar cells utilizing phenothiazine-based dyes, *Int. J. Photoenergy*, 2014, **2014**, 548914.
50 R. M. El-Shishtawy, *et al.*, Influence of redox electrolyte on the device performance of phenothiazine based dye sensitized solar cells, *New J. Chem.*, 2018, **42**(11), 9045–9050.
51 S. A. Al-horaibi, *et al.*, Indoline and benzothiazole-based squaraine dye-sensitized solar cells containing bis-pendent

sulfonate groups: Synthesis, characterization and solar cell performance, *J. Mol. Struct.*, 2019, **1195**, 591–597.

52 S. A. Al-horaibi, *et al.*, Synthesis and characterization of new squaraine dyes with bis-pendent carboxylic groups for dye-sensitized solar cells, *J. Mol. Struct.*, 2019, **1195**, 850–858.

53 C. Yang, *et al.*, Photovoltaic performance and power conversion efficiency prediction of double fence porphyrins, *Phys. Chem. Chem. Phys.*, 2021, **23**(47), 27042–27058.

54 K.-T. Wong, Intramolecular or Intermolecular Charge Transfer Approaches for Highly Efficient TADF Materials and OLEDs, in *Asia Communications and Photonics Conference*, Optical Society of America, 2017.

55 X. Ouyang, *et al.*, Effective management of intramolecular charge transfer to obtain from blue to violet-blue OLEDs based on a couple of phenanthrene isomers, *Dyes Pigm.*, 2015, **122**, 264–271.

56 M. A. Ei-Kemary, Photoinduced intramolecular charge transfer of 3-cyano-4-furyl-6-phenyl-2-(9-anthralylidene)-pyridine, *J. Photochem. Photobiol., A*, 2000, **137**(1), 9–14.

57 S. Muruganantham, *et al.*, Impact of tunable 2-(1 H-indol-3-yl) acetonitrile based fluorophores towards optical, thermal and electroluminescence properties, *RSC Adv.*, 2019, **9**(25), 14544–14557.

58 A. Ekbote, S. M. Mobin and R. Misra, Stimuli-responsive phenothiazine-based donor–acceptor isomers: AIE, mechanochromism and polymorphism, *J. Mater. Chem. C*, 2020, **8**(10), 3589–3602.

59 T. Gao, *et al.*, A self-assembled fluorescent organic nanoprobe and its application for sulfite detection in food samples and living systems, *Org. Biomol. Chem.*, 2017, **15**(20), 4375–4382.

60 S. M. J. Nabavi, *et al.*, Design, Synthesis and Application of Imidazole-Based Organic Dyes in Dye Sensitized Solar Cells, *J. Electron. Mater.*, 2020, **49**(6), 3735–3750.

61 J. Sivanadanam, I. S. Aidhen and K. Ramanujam, New cyclic and acyclic imidazole-based sensitizers for achieving highly efficient photoanodes for dye-sensitized solar cells by a potential-assisted method, *New J. Chem.*, 2020, **44**(25), 10207–10219.

62 S. Sambathkumar, *et al.*, Design and synthesis of imidazole-triphenylamine based organic materials for dye sensitized solar cells, *Mater. Lett.*, 2019, **242**, 28–31.

63 C. Reichardt and T. Welton, *Solvents and solvent effects in organic chemistry*, John Wiley & Sons, 2010.

64 A. M. Brouwer, *Standards for photoluminescence quantum yield measurements in solution* (IUPAC Technical Report), *Pure Appl. Chem.*, 2011, **83**, 2213–2228.

65 M. M. Haj, M. J. Chaichi and M. Yousefpour, Solvatochromism effect of different solvents on UV-Vis spectra of fluorescein and its derivatives, *Iran. J. Chem. Chem. Eng.*, 2008, **27**, 9–14.

66 A. Ekbote, T. Jadhav and R. Misra, T-Shaped donor–acceptor–donor type tetraphenylethylene substituted quinoxaline derivatives: aggregation-induced emission and mechanochromism, *New J. Chem.*, 2017, **41**(17), 9346–9353.

67 H.-X. Yu, *et al.*, Donor–acceptor type aggregation-induced emission luminophores based on the 1,1-dicyanomethylene-3-indanone unit for bridge-dependent reversible mechanochromism and light-up biosensing of hypochlorites, *J. Mater. Chem. C*, 2019, **7**(29), 8888–8897.

68 K. A. N. Upamali, *et al.*, Carbazole-Based Cyano-Stilbene Highly Fluorescent Microcrystals, *Langmuir*, 2011, **27**, 1573–1580.

69 M. Y. Abdelaal, T. R. Sobahi and R. M. El-Shishtawy, Chromophoric thin film based on cellulose triacetate blends for sensing metal ions, *C. R. Chim.*, 2014, **17**(6), 557–562.

70 D. Cheng, *et al.*, High contrast mechanochromic luminescence of aggregation-induced emission (AIE)-based 9,9-dimethyl-9,10-dihydroacridine-containing cruciform luminophores, *Dyes Pigm.*, 2020, **173**, 107934.

71 T. Jadhav, *et al.*, Aggregation induced emission and mechanochromism in pyrenoimidazoles, *J. Mater. Chem. C*, 2015, **3**(38), 9981–9988.

72 H. Zhang, *et al.*, Multi-purpose barbituric acid derivatives with aggregation induced emission, *Spectrochim. Acta, Part A*, 2019, **223**, 117320.

73 N. Nagarajan, *et al.*, Tunable single and dual emission behavior of imidazole fluorophores based on D-π-A architecture, *J. Photochem. Photobiol., A*, 2014, **284**, 36–48.

74 A. Vlček Jr and S. Záliš, Modeling of charge-transfer transitions and excited states in d6 transition metal complexes by DFT techniques, *Coord. Chem. Rev.*, 2007, **251**(3–4), 258–287.

75 D. L. Ashford, *et al.*, Controlling ground and excited state properties through ligand changes in ruthenium polypyridyl complexes, *Inorg. Chem.*, 2014, **53**(11), 5637–5646.

76 M. Cossi, *et al.*, Ab initio study of ionic solutions by a polarizable continuum dielectric model, *Chem. Phys. Lett.*, 1998, **286**(3–4), 253–260.

77 C. Adamo and V. Barone, Toward reliable density functional methods without adjustable parameters: The PBE0 model, *J. Chem. Phys.*, 1999, **110**(13), 6158–6170.